

Efficient tensor network algorithm for layered systems

Patrick C.G. Vlaar* and Philippe Corboz

*Institute for Theoretical Physics and Delta Institute for Theoretical Physics,
University of Amsterdam, Science Park 904, 1098 XH Amsterdam, The Netherlands*

(Dated: August 16, 2022)

Strongly correlated layered 2D systems are of central importance in condensed matter physics, but their numerical study is very challenging. Motivated by the enormous successes of tensor networks for 1D and 2D systems, we develop an efficient tensor network approach based on infinite projected entangled-pair states (iPEPS) for layered 2D systems. Starting from an anisotropic 3D iPEPS ansatz, we propose a contraction scheme in which the weakly-entangled layers are effectively decoupled away from the center of the layers, such that they can be efficiently contracted using 2D contraction methods while keeping the center of the layers connected in order to capture the most relevant interlayer correlations. We present benchmark data for the anisotropic 3D Heisenberg model on a cubic lattice, which show close agreement with quantum Monte Carlo and full 3D contraction results.

Understanding the emergent phenomena in strongly correlated systems is of central importance in modern physics. Among the most powerful tools to study these systems are tensor network (TN) methods, with the density matrix renormalization group (DMRG) [1] algorithm and its underlying variational ansatz, the matrix product state (MPS) [2, 3], being the best-known examples for (quasi) one-dimensional systems. Projected entangled-pair states (PEPS) [4, 5] (or tensor product states [6–8]) provide a natural generalization of MPS to higher dimensions. Thanks to algorithmic advances in the past years, PEPS has become a versatile state-of-the-art tool for 2D systems, not only for ground states [9–26], but also for finite temperature calculations [27–37], excited states [38–41], open systems [31, 42–44], and real-time evolution [31, 45–50]. 3D TN algorithms are more challenging because of their higher complexity, although progress has recently been made in developing methods with a tractable computational cost [51] (see also related works on 3D classical systems [52–57]).

A special and highly relevant class of 3D quantum systems is formed by layered 2D systems, in which the effective intralayer couplings are much stronger than the interlayer ones. Important realizations include the cuprate high- T_c superconductors [58] as well as various quasi-2D frustrated magnets such as Kagomé [59], triangular [60–64], Shastry-Sutherland [65–67], and honeycomb lattice compounds [68–71]. While pure 2D models often already capture the relevant physics of these systems, the interlayer couplings can play an important role on the quantitative level. For example, they lead to a finite Néel transition temperature in layered square lattice Heisenberg models as opposed to the pure 2D case, or they may play a significant role in the competition of low-energy states in the 2D Hubbard model [12]. Thus, accurate TN approaches to study these systems would be highly desirable.

In this letter, we introduce an efficient TN algorithm for layered 2D systems, called the layered corner transfer

matrix (LCTM) method, which is substantially simpler and computationally cheaper than full 3D approaches. Motivated by the layered nature of these systems, we start from an anisotropic PEPS ansatz, i.e., with a small interlayer bond dimension D_z compared to the intralayer bond dimension D_{xy} , which control the accuracy of the ansatz. The main idea of the algorithm is to contract the 3D TN by (1) performing an effective decoupling of the layers away from the center of each layer, (2) contracting the individual decoupled layers using the standard 2D corner transfer matrix (CTM) method [10, 72, 73], and (3) contracting the remaining TN, formed by the contracted layers connected with a finite bond dimension $D_z > 1$ in the center of each layer. A core ingredient of the approach is the effective decoupling procedure which we implement based on an iterative full update (FU) truncation scheme [74, 75]. We present benchmark results for the anisotropic Heisenberg model on a cubic lattice, which show close agreement with a full 3D contraction and with quantum Monte Carlo (QMC) data already for small D_z . Finally, we highlight directions for future improvements and extensions of the LCTM approach.

Method. — We consider an infinite PEPS (iPEPS), shown in Fig. 1(a), consisting of a tensor (or more generally a unit cell of tensors) that is repeated on the infinite cubic lattice. Each tensor has 7 indices: one physical index carrying the local Hilbert space of a site, four indices with bond dimension D_{xy} connecting to the intraplane nearest-neighbor tensors, and two indices of dimension D_z connecting to the tensors in the neighboring planes. The accuracy of the ansatz is systematically controlled by D_{xy} and D_z , where we choose $D_{xy} \geq D_z$ motivated by the anisotropic nature of layered 2D systems. In the limit of $D_z = 1$, the ansatz corresponds to a product state of 2D iPEPS layers, i.e., a state without entanglement between the layers (but with entanglement within the layers, controlled by D_{xy}).

The main challenge of a 3D TN algorithm is the effi-

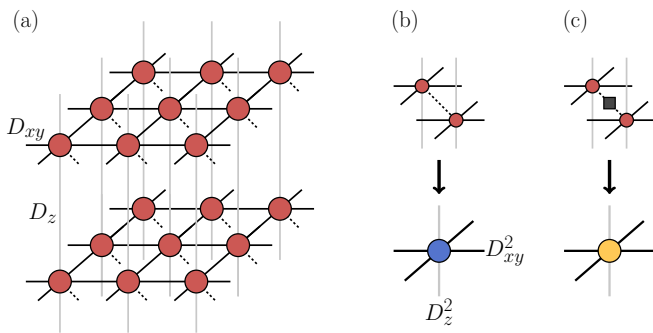


FIG. 1. (a) Anisotropic 3D iPEPS ansatz with intralayer and interlayer bond dimensions D_{xy} and D_z , respectively. In the limit $D_z = 1$ the ansatz reduces to a product of decoupled iPEPS layers. (b) The norm tensor is obtained by contracting the bra- and ket-tensors on each site and combining pairs of auxiliary indices into new auxiliary indices with dimensions D_{xy}^2 and D_z^2 , respectively. (c) Same as in (b) but with a local operator between the bra- and ket-tensors for the evaluation of a local expectation value.

cient, approximate contraction of the 3D TN, which is needed to compute, e.g., a local expectation value. Let us consider computing the norm of the wave function. The corresponding TN is depicted in Fig. 2(a), where the bra- and ket-tensors on each site are contracted as shown in Fig. 1(b). To compute a local expectation value, we can simply put an operator between the local tensors as shown in Fig. 1(c) and replace the norm tensor by this new tensor at the desired location.

In the simplest case, for $D_z = 1$, this network consists of independent 2D square lattice networks which can be efficiently contracted using the CTM method [10, 72, 73]. The CTM method is an iterative approach that approximates the 2D TN surrounding a central tensor by a set of environment tensors, given by four corner and four edge tensors (shown by the black disc-shaped tensors in Fig. 2(c)), where the accuracy is systematically controlled by the boundary bond dimension χ of the environment tensors.

For the case $D_z > 1$, a full 3D contraction algorithm as in Ref. [51] could be used. This, however, is computationally expensive, and we thus follow a more efficient strategy here, exploiting the anisotropic nature of the ansatz. The main idea is to project the vertical indices away from the center of each layer onto $D_z = 1$ (see details below), while keeping the full bond dimension $D_z > 1$ on the tensors in the center, see Fig. 2(b). This leads to an effective decoupling of the 2D layers away from the center, such that the standard 2D CTM approach can be used to contract them (Fig. 2(c)) while the most relevant interlayer correlations are still taken into account by the vertical connections of the tensors in the center. Since the bonds in the z -direction carry only little entanglement, the projection onto $D_z = 1$ away from the center is expected to induce only a small error on a local expectation value

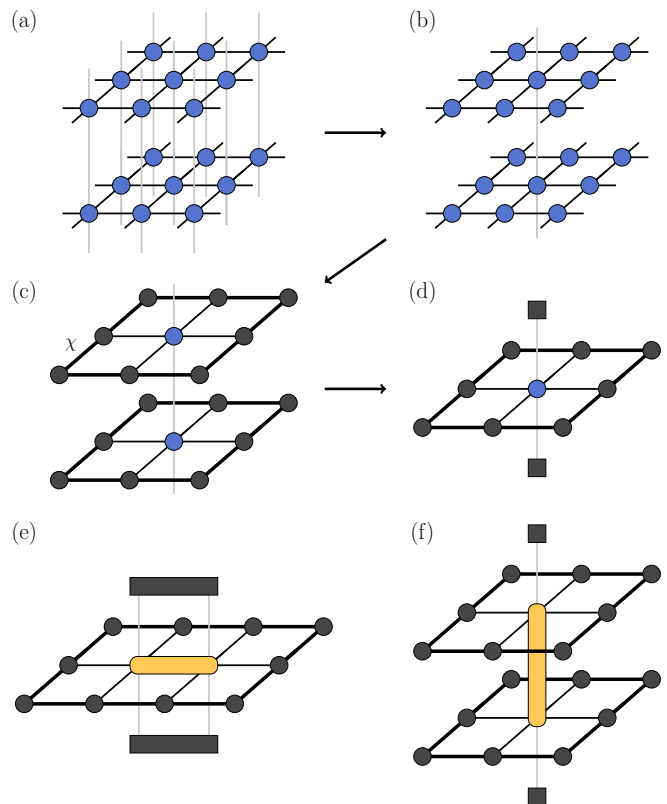


FIG. 2. The main steps of the LCTM contraction method. (a) 3D TN representing the norm. (b) TN with decoupled layers away from the center, obtained by a projection of the vertical indices in (a) onto $D_z = 1$ (except in the center). (c) The decoupled 2D layers are contracted using the CTM method, which yields the environment tensors around the central tensor, i.e., four corner and four edge tensors (in black), with an accuracy controlled by the boundary bond dimension χ . (d) The infinite central chain with contracted layers can be evaluated by replacing the neighboring layers by the left- and right-dominant eigenvector (black squares) of the transfer matrix represented by a contracted layer. A local expectation value can be computed by replacing the central norm tensor by the yellow tensor shown in Fig. 1(c). (e)-(f) Relevant diagrams to compute intra- and interlayer nearest-neighbor observables, where the yellow tensor is obtained from contracting neighboring bra- and ket-tensors with a 2-site operator in between.

measured in the center. After contracting each layer, the resulting TN corresponds to an infinite 1D chain in the vertical direction with bond dimension D_z^2 , which can be evaluated by sandwiching the central layer between the left- and right-dominant eigenvector of the corresponding transfer matrix (represented by a contracted layer), as shown in Fig. 2(d).

A core ingredient of the algorithm is the projection step from $D_z > 1$ to $D_z = 1$, which we discuss in the following. Here, we use a scheme based on a full update (FU) truncation [74, 75], a technique that is also applied in the context of imaginary time evolution algorithms to

truncate a bond index in an iPEPS. It is based on a minimization of the norm distance, $d = \|\psi - \psi'\|^2$, which can be solved iteratively, where $|\psi\rangle$ is the untruncated iPEPS and $|\psi'\rangle$ is the iPEPS with one bond truncated down to $D_z = 1$. The FU does, however, require the environment tensors, which we initially do not have. We thus start from an initial approximate projection based on the simple update (SU) approach [76], which only considers local tensors for the truncation, from which the environment for the FU projection is computed. To improve the accuracy of the truncation, one can repeat the computation of the environment iteratively. In practice, for the model considered here, we found that one FU iteration is sufficient to reach convergence. For a discussion of other truncation approaches, see the supplemental material [77].

The accuracy of the LCTM method is controlled by the boundary bond dimension χ and by the number of $D_z > 1$ connections we keep in the center. Here, we focus on the simplest case, where we only keep the connections on the central tensor for the evaluation of one-site observables and interplane two-site observables (see Fig. 2(f)), which we find is sufficient in the limit of weak interlayer coupling, as we will show in our benchmark results. For intralayer two-site observables we keep two connections, as depicted in Fig. 2(e). The computational cost of these contractions are $\chi^3 D_{xy}^4 + \chi^2 D_{xy}^6 D_z^2$ and $\min[\chi^3 D_{xy}^6, \chi^3 D_{xy}^4 D_z^4]$, respectively. In the supplemental material [77] we also consider a scheme with more connections, which is more accurate, but also computationally more expensive.

The LCTM contraction method can not only be used for the computation of observables, but also in combination with accurate optimization schemes (to find the optimal variational parameters in the tensors for a given Hamiltonian), e.g., in an imaginary time evolution with fast full update (FFU) [75] or in energy minimization algorithms [78–80]. We further note that the LCTM method can be extended to arbitrary unit cell sizes in a similar way to the standard CTM in 2D [10, 81].

Results. — To benchmark the method, we consider the anisotropic 3D Heisenberg model on a cubic lattice given by the Hamiltonian

$$\hat{H} = J_{xy} \sum_{\langle ij \rangle_{xy}} \mathbf{S}_i \mathbf{S}_j + J_z \sum_{\langle ij \rangle_z} \mathbf{S}_i \mathbf{S}_j, \quad (1)$$

with J_{xy} the intralayer and J_z the interlayer coupling strengths and \mathbf{S}_i spin $S = 1/2$ operators. We use an iPEPS ansatz with two tensors, one for each sublattice, to capture the long-range antiferromagnetic order. The iPEPS is optimized with the FFU imaginary time evolution algorithm [75], starting from initial tensors obtained with simple update optimization [76] (see the supplemental material [77] for results with different optimization methods). In the CTM approach, we keep a sufficiently

large boundary bond dimension χ , such that finite- χ effects are negligible (see the supplemental material [77]). To improve the computational efficiency, tensors with implemented $U(1)$ symmetry [82, 83] are used. We compare our results to ones computed with the full 3D contraction approach (SU+CTM) from Ref. [51] and with QMC results based on the directed loop algorithm from the ALPS library [84, 85] (obtained at a sufficiently low temperature of $T = 0.005 J_{xy}$). To extrapolate the QMC data to the thermodynamic limit, a finite size scaling analysis is performed using the scaling relations for the isotropic 3D Heisenberg model on the cubic lattice from Ref. [86] for lattices of size $L \times L \times L/2$ with L up to 20 for $J_z/J_{xy} = 0.05$ and 0.1, and with $L \times L \times L$ lattices for a maximum L of 12 for $J_z/J_{xy} = 0.2$.

We first consider the results for the energy per site, e , for $J_z/J_{xy} = 0.1$ in Fig. 3(a), plotted as a function of inverse bond dimension D_{xy} for different values of D_z . Already a product of iPEPS layers ($D_z = 1$) yields a value that is remarkably close to the extrapolated QMC result, with a relative error of only 0.15% for $D_{xy} = 6$. When D_z is increased to 2, a significant improvement is found and the relative error at $D_{xy} = 6$ is reduced to 0.05%, while a further increase to $D_z = 3$ only yields a small enhancement. Overall, the improvement of the variational energy is clearly larger when increasing D_{xy} (at least up to 4) compared to the improvement when increasing D_z , which further motivates the use of an anisotropic ansatz with $D_{xy} > D_z$. Comparing the LCTM scheme with the full 3D contraction (SU+CTM) only a small difference between the two methods is found.

Results for the local magnetic moment m are shown in Fig. 3(b). Whereas m systematically approaches the extrapolated QMC result with increasing D_{xy} , the dependence on D_z is small, suggesting that the reduction of the magnetic moment is predominantly due to the intraplane quantum fluctuations. The relative error of m at $D_{xy} = 6$ and $D_z = 3$ is 1.7(1)%. In Fig. 3(c) we present results for the nearest-neighbor spin-spin correlators in the intraplane and z -direction. The former is more accurately reproduced, which is a natural consequence of the fact that the latter enters with a prefactor $J_z/J_{xy} = 0.1$ in the optimization of the tensors. Still, we find that the extrapolated QMC result is approached with increasing D_z at large D_{xy} (note that increasing the two bond dimensions has an opposite effect on the change in the $\langle \mathbf{S}\mathbf{S} \rangle_z$ correlator).

In Fig. 4 we present results for the energy per site as a function of J_z/J_{xy} , for selected values of D_{xy} and D_z . Starting with the data for $D_{xy} = 3$ and $D_z = 2$ we find that the deviation with respect to the SU+CTM result slightly increases with increasing J_z/J_{xy} , although the deviation remains small even at a relatively large value of $J_z/J_{xy} = 0.2$. For a small ratio $J_z/J_{xy} = 0.05$, a product of iPEPS layers ($D_z = 1$) for $D_{xy} = 6$ already provides an energy close to the extrapolated QMC result,

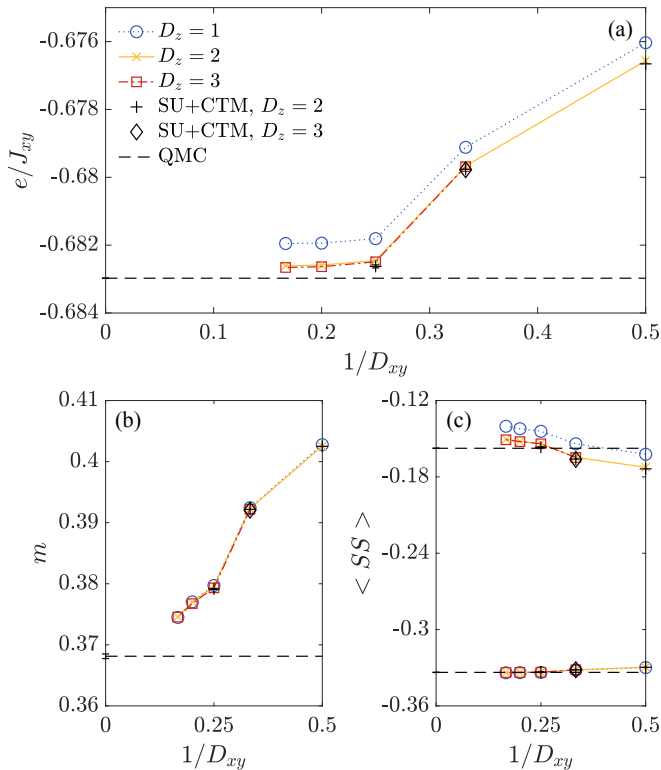


FIG. 3. Results for the anisotropic 3D Heisenberg model with $J_z/J_{xy} = 0.1$ as a function of $1/D_{xy}$, obtained for $D_z = 1 - 3$. For comparison, the extrapolated QMC results are indicated by the horizontal dashed lines with the error bars shown on the y-axis. Data based on the full 3D contraction approach (SU+CTM) is shown by the black symbols. (a) Energy per site e in units of J_{xy} . (b) Local magnetic moment m . (c) Nearest-neighbor spin-spin correlator in the z -direction, $\langle SS \rangle_z$ (top), and in the xy -direction, $\langle SS \rangle_{xy}$ (bottom).

with only a small improvement when increasing D_z to 2. In contrast, for $J_z/J_{xy} = 0.2$ the energy gain is large when increasing D_z , which is a natural consequence of the stronger entanglement between the layers for larger interlayer coupling.

To further motivate the anisotropic ansatz and contraction approach, let us consider the singular value spectrum on the intraplane and interplane bonds in Fig. 4. The singular values are naturally obtained in the SU optimization algorithm [76] which is based on local singular value decompositions. Here, we extracted them from our FFU-optimized tensors using the algorithm from Ref. [87]. A much faster decay of the singular values can be observed in the z -direction than in the intraplane direction, as expected, due to the weak entanglement between the planes. Increasing J_z/J_{xy} leads to a slower decay in the z -direction, suggesting that the value of D_z needs to be increased. Eventually, for sufficiently large J_z/J_{xy} the singular values in all directions will become

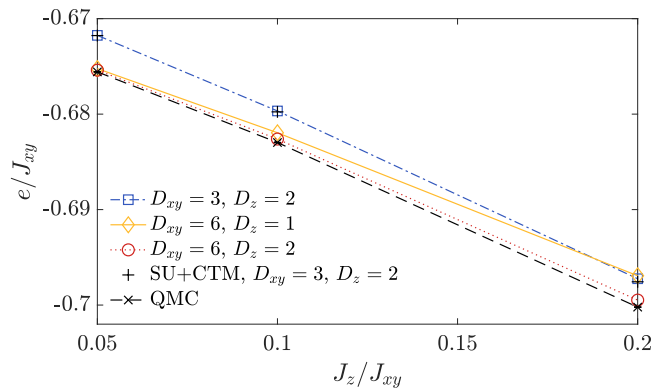


FIG. 4. Energy per site as a function of J_z/J_{xy} for different sets of bond dimensions, in comparison with data from a full 3D contraction (SU+CTM) and extrapolated QMC results.

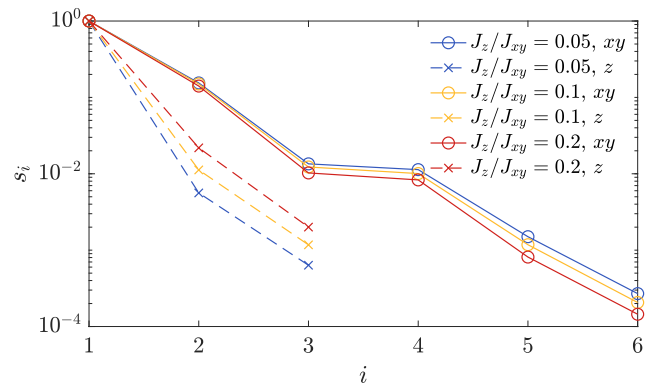


FIG. 5. Spectrum of the singular values s_i on the intra- and interplane bonds in the iPEPS ansatz obtained for $D_{xy} = 6$ and $D_z = 3$, exhibiting a fast decay (weak entanglement) in the z -direction and a slow decay (strong entanglement) in the xy -direction for small J_z/J_{xy} .

of similar magnitude, such that an anisotropic ansatz in combination with the LCTM contraction is no longer justified.

Conclusions. — We have introduced the LCTM method which is an efficient approach to study layered 2D systems with a weak interlayer coupling. The main idea is to perform a decoupling of the 3D network using the FU truncation onto $D_z = 1$ away from the center of each plane, while keeping the full bond dimension $D_z > 1$ in the center, such that the resulting network can be efficiently contracted with the standard CTM method in each layer. Our benchmark results for the anisotropic Heisenberg model demonstrate that the method yields values in close agreement with a full 3D contraction (SU+CTM), at a substantially lower computational cost. The results are close to the extrapolated QMC result even for a small interlayer bond dimension $D_z = 2$. Although the accuracy decreases when J_z/J_{xy} is increased, errors remain relatively small up to $J_z/J_{xy} = 0.2$.

There are several promising ways to further improve

the LCTM method. First, the accuracy of the FU projection onto $D_z = 1$ could be improved by making use of disentanglers between the layers [88, 89]. Second, the accuracy of the contraction can be increased by including more $D_z > 1$ bonds in the center (see the supplemental material [77]), although at a higher computational cost. Instead of keeping k open legs with total bond dimension $(D_z)^k$ in between the layers, the total dimension could be effectively reduced by introducing appropriate projectors between the layers. Third, instead of a complete decoupling away from the center, a small vertical bond dimension χ_z could be kept in the CTM environment tensors in order to capture the most relevant interlayer entanglement away from the center. And finally, the contraction scheme may also be combined with an energy minimization based on automatic differentiation [80] which is expected to provide more accurate tensors than the FFU optimization used here.

We believe our approach provides a powerful and practical tool for future studies of challenging layered 2D systems, especially models that are out of reach of QMC due to the negative sign problem. Finally, we note that the LCTM method can be straightforwardly extended to fermionic systems and finite temperature calculations, e.g., by adapting ideas from Refs. [90–93] and Refs. [30, 31], respectively.

This project has received funding from the European Research Council (ERC) under the European Union’s Horizon 2020 research and innovation programme (grant agreement Nos. 677061 and 101001604). This work is part of the D-ITP consortium, a program of the Netherlands Organization for Scientific Research (NWO) that is funded by the Dutch Ministry of Education, Culture, and Science (OCW).

* p.c.g.vlaar@uva.nl

- [1] S. R. White, Phys. Rev. Lett. **69**, 2863 (1992).
- [2] M. Fannes, B. Nachtergaele, and R. F. Werner, Commun. Math. Phys. **144**, 443 (1992).
- [3] S. Östlund and S. Rommer, Phys. Rev. Lett. **75**, 3537 (1995).
- [4] F. Verstraete and J. I. Cirac, arXiv:cond-mat/0407066 (2004).
- [5] V. Murg, F. Verstraete, and J. I. Cirac, Phys. Rev. A **75**, 033605 (2007).
- [6] Y. Hieida, K. Okunishi, and Y. Akutsu, New J. Phys. **1**, 7.1 (1999).
- [7] N. Maeshima, Y. Hieida, Y. Akutsu, T. Nishino, and K. Okunishi, Phys. Rev. E **64**, 016705 (2001).
- [8] Y. Nishio, N. Maeshima, A. Gendiar, and T. Nishino, arXiv:cond-mat/0401115 (2004).
- [9] P. Corboz and F. Mila, Phys. Rev. Lett. **112**, 147203 (2014).
- [10] P. Corboz, T. M. Rice, and M. Troyer, Phys. Rev. Lett. **113**, 046402 (2014).
- [11] H. J. Liao, Z. Y. Xie, J. Chen, Z. Y. Liu, H. D. Xie, R. Z. Huang, B. Normand, and T. Xiang, Phys. Rev. Lett. **118**, 137202 (2017).
- [12] B.-X. Zheng, C.-M. Chung, P. Corboz, G. Ehlers, M.-P. Qin, R. M. Noack, H. Shi, S. R. White, S. Zhang, and G. K.-L. Chan, Science **358**, 1155 (2017).
- [13] I. Niesen and P. Corboz, Phys. Rev. B **95**, 180404 (2017).
- [14] J.-Y. Chen, L. Vanderstraeten, S. Capponi, and D. Poilblanc, Phys. Rev. B **98**, 184409 (2018).
- [15] S. S. Jahromi and R. Orús, Phys. Rev. B **98**, 155108 (2018).
- [16] H.-Y. Lee and N. Kawashima, Phys. Rev. B **97**, 205123 (2018).
- [17] H. Yamaguchi, Y. Sasaki, T. Okubo, M. Yoshida, T. Kida, M. Hagiwara, Y. Kono, S. Kittaka, T. Sakakibara, M. Takigawa, Y. Iwasaki, and Y. Hosokoshi, Phys. Rev. B **98**, 094402 (2018).
- [18] B. Ponsioen, S. S. Chung, and P. Corboz, Phys. Rev. B **100**, 195141 (2019).
- [19] A. Kshetrimayum, C. Balz, B. Lake, and J. Eisert, Ann. Phys. (N. Y.) **421**, 168292 (2020).
- [20] S. S. Chung and P. Corboz, Phys. Rev. B **100**, 035134 (2019).
- [21] R. Haghshenas, S.-S. Gong, and D. N. Sheng, Phys. Rev. B **99**, 174423 (2019).
- [22] J.-Y. Chen, S. Capponi, A. Wietek, M. Mambrini, N. Schuch, and D. Poilblanc, Phys. Rev. Lett. **125**, 017201 (2020).
- [23] H.-Y. Lee, R. Kaneko, L. E. Chern, T. Okubo, Y. Yamaji, N. Kawashima, and Y. B. Kim, Nat. Commun. **11**, 1639 (2020).
- [24] O. Gauthé, S. Capponi, M. Mambrini, and D. Poilblanc, Phys. Rev. B **101**, 205144 (2020).
- [25] J. Hasik, D. Poilblanc, and F. Becca, SciPost Phys. **10**, 012 (2021).
- [26] W.-Y. Liu, J. Hasik, S.-S. Gong, D. Poilblanc, W.-Q. Chen, and Z.-C. Gu, arXiv:2110.11138 [cond-mat.str-el] (2021).
- [27] P. Czarnik, J. Dziarmaga, and A. M. Oleś, Phys. Rev. B **96**, 014420 (2017).
- [28] C. Peng, S.-J. Ran, T. Liu, X. Chen, and G. Su, Phys. Rev. B **95**, 075140 (2017).
- [29] X. Chen, S.-J. Ran, T. Liu, C. Peng, Y.-Z. Huang, and G. Su, Sci. Bull. **63**, 1545 (2018).
- [30] A. Kshetrimayum, M. Rizzi, J. Eisert, and R. Orús, Phys. Rev. Lett. **122**, 070502 (2019).
- [31] P. Czarnik, J. Dziarmaga, and P. Corboz, Phys. Rev. B **99**, 035115 (2019).
- [32] A. Wietek, P. Corboz, S. Wessel, B. Normand, F. Mila, and A. Honecker, Phys. Rev. Res. **1**, 033038 (2019).
- [33] P. Czarnik, A. Francuz, and J. Dziarmaga, Phys. Rev. B **100**, 165147 (2019).
- [34] P. Czarnik, M. M. Rams, P. Corboz, and J. Dziarmaga, Phys. Rev. B **103**, 075113 (2021).
- [35] J. L. Jiménez, S. P. G. Crone, E. Fogh, M. E. Zayed, R. Lortz, E. Pomjakushina, K. Conder, A. M. Läuchli, L. Weber, S. Wessel, A. Honecker, B. Normand, C. Rüegg, P. Corboz, H. M. Rønnow, and F. Mila, Nature **592**, 370 (2021).
- [36] D. Poilblanc, M. Mambrini, and F. Alet, SciPost Phys. **10**, 019 (2021).
- [37] O. Gauthé and F. Mila, Phys. Rev. Lett. **128**, 227202 (2022).
- [38] L. Vanderstraeten, J. Haegeman, and F. Verstraete,

- Phys. Rev. B **99**, 165121 (2019).
- [39] B. Ponsioen and P. Corboz, Phys. Rev. B **101**, 195109 (2020).
- [40] B. Ponsioen, F. Assaad, and P. Corboz, SciPost Phys. **12**, 006 (2022).
- [41] R.-Z. Chi, Y. Liu, Y. Wan, H.-J. Liao, and T. Xiang, arXiv:2201.12121 [cond-mat.str-el] (2022).
- [42] A. Kshetrimayum, H. Weimer, and R. Orús, Nat. Commun. **8**, 1291 (2017).
- [43] D. Kilda, A. Biella, M. Schiro, R. Fazio, and J. Keeling, SciPost Physics Core **4**, 005 (2021).
- [44] C. Mc Keever and M. H. Szymańska, Phys. Rev. X **11**, 021035 (2021).
- [45] C. Hubig and J. I. Cirac, SciPost Phys. **6**, 31 (2019).
- [46] C. Hubig, A. Bohrdt, M. Knap, F. Grusdt, and J. I. Cirac, SciPost Phys. **8**, 21 (2020).
- [47] A. Kshetrimayum, M. Goihl, and J. Eisert, Phys. Rev. B **102**, 235132 (2020).
- [48] A. Kshetrimayum, M. Goihl, D. M. Kennes, and J. Eisert, Phys. Rev. B **103**, 224205 (2021).
- [49] M. Schmitt, M. M. Rams, J. Dziarmaga, M. Heyl, and W. H. Zurek, arXiv:2106.09046 [cond-mat.str-el] (2021).
- [50] J. Dziarmaga, Phys. Rev. B **105**, 054203 (2022).
- [51] P. C. G. Vlaar and P. Corboz, Phys. Rev. B **103**, 205137 (2021).
- [52] T. Nishino and K. Okunishi, J. Phys. Soc. Jpn. **67**, 3066 (1998).
- [53] T. Nishino, K. Okunishi, Y. Hieida, N. Maeshima, and Y. Akutsu, Nucl. Phys. B **575**, 504 (2000).
- [54] T. Nishino, Y. Hieida, K. Okunishi, N. Maeshima, Y. Akutsu, and A. Gendiar, Prog. Theor. Phys. **105**, 409 (2001).
- [55] Z. Y. Xie, J. Chen, M. P. Qin, J. W. Zhu, L. P. Yang, and T. Xiang, Phys. Rev. B **86**, 045139 (2012).
- [56] R. Orús, Phys. Rev. B **85**, 205117 (2012).
- [57] L. Vanderstraeten, B. Vanhecke, and F. Verstraete, Phys. Rev. E **98**, 042145 (2018).
- [58] J. G. Bednorz and K. A. Müller, Z. Phys. B **64**, 189 (1986).
- [59] M. P. Shores, E. A. Nytko, B. M. Bartlett, and D. G. Nocera, J. Am. Chem. Soc. **127**, 13462 (2005).
- [60] R. Coldea, D. A. Tennant, A. M. Tsvelik, and Z. Tylczynski, Phys. Rev. Lett. **86**, 1335 (2001).
- [61] Y. Shimizu, K. Miyagawa, K. Kanoda, M. Maesato, and G. Saito, Phys. Rev. Lett. **91**, 107001 (2003).
- [62] Y. Shirata, H. Tanaka, A. Matsuo, and K. Kindo, Phys. Rev. Lett. **108**, 057205 (2012).
- [63] R. Rawl, L. Ge, H. Agrawal, Y. Kamiya, C. R. Dela Cruz, N. P. Butch, X. F. Sun, M. Lee, E. S. Choi, J. Oitmaa, C. D. Batista, M. Mourigal, H. D. Zhou, and J. Ma, Phys. Rev. B **95**, 060412 (2017).
- [64] Y. Cui, J. Dai, P. Zhou, P. S. Wang, T. R. Li, W. H. Song, J. C. Wang, L. Ma, Z. Zhang, S. Y. Li, G. M. Luke, B. Normand, T. Xiang, and W. Yu, Phys. Rev. Materials **2**, 044403 (2018).
- [65] H. Kageyama, K. Yoshimura, R. Stern, N. V. Mushnikov, K. Onizuka, M. Kato, K. Kosuge, C. P. Slichter, T. Goto, and Y. Ueda, Phys. Rev. Lett. **82**, 3168 (1999).
- [66] S. Miyahara and K. Ueda, Phys. Rev. Lett. **82**, 3701 (1999).
- [67] S. Miyahara and K. Ueda, J. Phys.: Condens. Matter **15**, R327 (2003).
- [68] Y. Singh and P. Gegenwart, Phys. Rev. B **82**, 064412 (2010).
- [69] K. W. Plumb, J. P. Clancy, L. J. Sandilands, V. V. Shankar, Y. F. Hu, K. S. Burch, H.-Y. Kee, and Y.-J. Kim, Phys. Rev. B **90**, 041112 (2014).
- [70] H. Takagi, T. Takayama, G. Jackeli, G. Khaliullin, and S. E. Nagler, Nat Rev Phys **1**, 264 (2019).
- [71] C. Wessler, B. Roessli, K. W. Krämer, B. Delley, O. Waldmann, L. Keller, D. Cheptiakov, H. B. Braun, and M. Kenzelmann, npj Quantum Mater. **5**, 85 (2020).
- [72] T. Nishino and K. Okunishi, J. Phys. Soc. Jpn. **65**, 891 (1996).
- [73] R. Orús and G. Vidal, Phys. Rev. B **80**, 094403 (2009).
- [74] J. Jordan, R. Orús, G. Vidal, F. Verstraete, and J. I. Cirac, Phys. Rev. Lett. **101**, 250602 (2008).
- [75] H. N. Phien, J. A. Bengua, H. D. Tuan, P. Corboz, and R. Orús, Phys. Rev. B **92**, 035142 (2015).
- [76] H. C. Jiang, Z. Y. Weng, and T. Xiang, Phys. Rev. Lett. **101**, 090603 (2008).
- [77] See Supplemental Material for more technical details and additional data.
- [78] P. Corboz, Phys. Rev. B **94**, 035133 (2016).
- [79] L. Vanderstraeten, J. Haegeman, P. Corboz, and F. Verstraete, Phys. Rev. B **94**, 155123 (2016).
- [80] H.-J. Liao, J.-G. Liu, L. Wang, and T. Xiang, Phys. Rev. X **9**, 031041 (2019).
- [81] P. Corboz, S. R. White, G. Vidal, and M. Troyer, Phys. Rev. B **84**, 041108 (2011).
- [82] S. Singh, R. N. C. Pfeifer, and G. Vidal, Phys. Rev. B **83**, 115125 (2011).
- [83] B. Bauer, P. Corboz, R. Orús, and M. Troyer, Phys. Rev. B **83**, 125106 (2011).
- [84] A. Albuquerque, F. Alet, P. Corboz, P. Dayal, A. Feiguin, S. Fuchs, L. Gamper, E. Gull, S. Gürtler, A. Honecker, R. Igarashi, M. Körner, A. Kozhevnikov, A. Läuchli, S. Manmana, M. Matsumoto, I. McCulloch, F. Michel, R. Noack, G. Pawłowski, L. Pollet, T. Pruschke, U. Schollwöck, S. Todo, S. Trebst, M. Troyer, P. Werner, and S. Wessel, J. Magn. Magn. Mater. **310**, 1187 (2007).
- [85] B. Bauer, L. D. Carr, H. G. Evertz, A. Feiguin, J. Freire, S. Fuchs, L. Gamper, J. Gukelberger, E. Gull, S. Guertler, A. Hehn, R. Igarashi, S. V. Isakov, D. Koop, P. N. Ma, P. Mates, H. Matsuo, O. Parcollet, G. Pawłowski, J. D. Picon, L. Pollet, E. Santos, V. W. Scarola, U. Schollwöck, C. Silva, B. Surer, S. Todo, S. Trebst, M. Troyer, M. L. Wall, P. Werner, and S. Wessel, J. Stat. Mech.: Theory Exp. **2011** (05), P05001.
- [86] P. Hasenfratz and F. Niedermayer, Z. Phys. B **92**, 91 (1993).
- [87] H. N. Phien, I. P. McCulloch, and G. Vidal, Phys. Rev. B **91**, 115137 (2015).
- [88] G. Vidal, Phys. Rev. Lett. **99**, 220405 (2007).
- [89] G. Evenbly and G. Vidal, Phys. Rev. Lett. **115**, 180405 (2015).
- [90] C. V. Kraus, N. Schuch, F. Verstraete, and J. I. Cirac, Phys. Rev. A **81**, 052338 (2010).
- [91] T. Barthel, C. Pineda, and J. Eisert, Phys. Rev. A **80**, 042333 (2009).
- [92] P. Corboz, R. Orus, B. Bauer, and G. Vidal, Phys. Rev. B **81**, 165104 (2010).
- [93] Z.-C. Gu, F. Verstraete, and X.-G. Wen, arXiv:1004.2563 [cond-mat.str-el] (2010).

Supplemental Material for "Efficient tensor network algorithm for layered systems"

Patrick C.G. Vlaar* and Philippe Corboz

*Institute for Theoretical Physics and Delta Institute for Theoretical Physics,
University of Amsterdam, Science Park 904, 1098 XH Amsterdam, The Netherlands*

(Dated: August 16, 2022)

In this supplemental material, additional details and results on the iPEPS optimization and the accuracy of the LCTM scheme are presented. In Sec. I, the optimization of the iPEPS is discussed, with additional details on the fast full update (FFU) approach and a comparison to other imaginary time evolution methods. Additional results on the accuracy and convergence of the LCTM are provided in Sec. II, including the dependence on the boundary bond dimension χ , the number of interlayer $D_z > 1$ connections, and a comparison of different layer decoupling procedures.

I. IMAGINARY TIME EVOLUTION WITH LCTM

In this section, we provide more details on the full update (FU) method [1, 2], which we use for the imaginary time evolution based optimization algorithm, as well as for the truncation of the interlayer bond $D_z > 1$ to $D_z = 1$ in the LCTM method.

The main idea of the imaginary time evolution algorithm is to project an initial state onto the ground state by applying the imaginary time evolution operator $e^{-\beta\hat{H}}$ with $\beta \rightarrow \infty$ on the initial state. By using the Trotter-Suzuki decomposition the operator is split into a product of local nearest-neighbor gates which are sequentially applied to the iPEPS ansatz. Each application of a gate increases the bond dimension between the two sites, which needs to be truncated to avoid an exponential growth of the bond dimension.

In the FU, the truncation of a bond is performed by minimizing the norm distance

$$\begin{aligned} d &= \|\psi - \psi'\|^2 \\ &= \langle \psi | \psi \rangle + \langle \psi' | \psi' \rangle - \langle \psi | \psi' \rangle - \langle \psi' | \psi \rangle \end{aligned} \quad (1)$$

with $|\psi\rangle$ the untruncated and $|\psi'\rangle$ the truncated iPEPS. The computation of the overlaps requires a contraction which we perform with the LCTM method. The relevant environments are shown in Fig. 1. To minimize the distance in Eq. 1 we insert a pair of projectors on the bond that needs to be truncated and we optimize them iteratively. To improve the stability of the algorithm, the norm matrix is explicitly made Hermitian and positive definite [3].

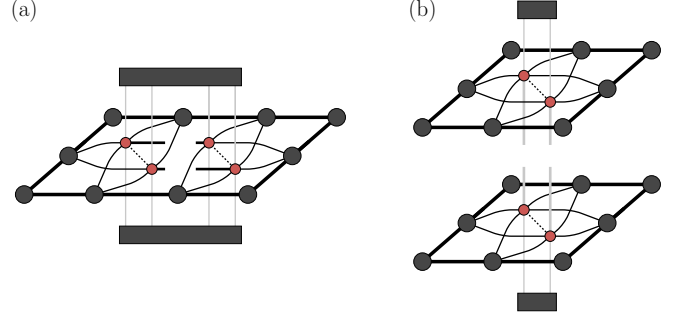


FIG. 1. The environments used in the FU imaginary time evolution. (a) Environment for the intraplane update steps. (b) Environment used in the interlayer direction.

The computational cost of this procedure is dominated by the contraction to obtain the environment which has to be computed every time a new gate is applied. To reduce the cost, we make use of the fast full update (FFU) [2]. In the FFU, instead of performing a full convergence of the environment with the CTM method after applying a gate, the environment from the previous time step is recycled, and only one single CTM iteration in the direction of the updated bond is performed, which is computationally cheaper. The FFU is motivated by the observation that an application of a single time-evolution gate with a small time step has typically only a small effect on the environment. In addition to the CTM environment tensors, we also recycle both the projectors that truncate the iPEPS tensors to $D_z \rightarrow 1$ as well as the dominant eigenvectors carrying contributions from the other layers that are used in the x- and y-update steps. Both are recomputed after the z-update steps.

A. Comparison to other imaginary time evolution methods

In this section, results from different imaginary time evolution methods are compared. Besides the FFU, we also consider the simple update (SU) [4], in which the truncation of a bond is done based on a local SVD. The SU is computationally considerably cheaper than the FFU, but also less accurate. We also present results obtained from a cluster update (CU) [3, 5–7], which takes only a finite number of tensors into account to minimize Eq. 1. Here we used the 4×3 cluster in intraplane update steps and the 3×3 cluster in the interplane direction shown in Figs. 2(c) and 2(d), respectively.

* p.c.g.vlaar@uva.nl

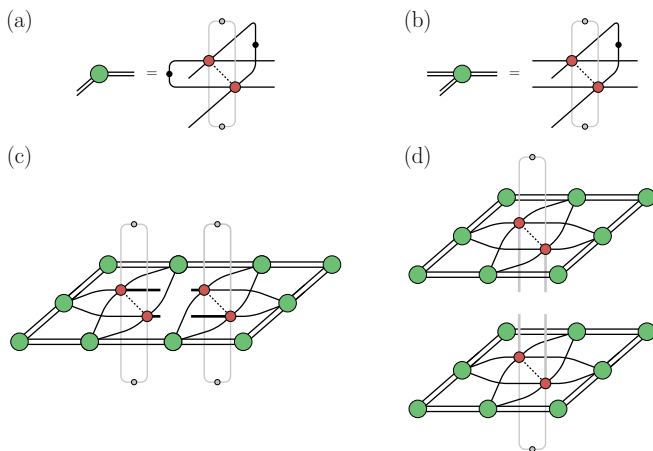


FIG. 2. The environments used in the CU imaginary time evolution. (a+b) For graphical brevity, a compact notation is used. The small circles on the traced-out bonds represent the corresponding singular value matrices on the bonds. (c) 4×3 cluster environment used for the intraplane update steps. (d) 3×3 environment used in the interplane direction.

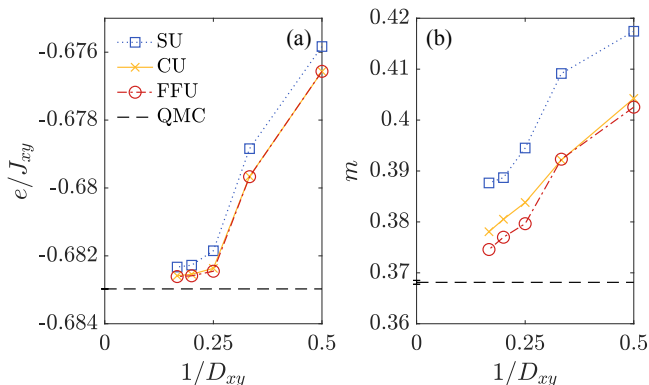


FIG. 3. Comparison of results obtained with different imaginary time evolution methods with $J_z/J_{xy} = 0.1$ as a function of $1/D_{xy}$ and $D_z = 2$. (a) Energy per site e in units of J_{xy} . (b) Local magnetic moment m .

Figure 3(a) shows the energy per site e as a function of $1/D_{xy}$ obtained with the different imaginary time evolution schemes for the anisotropic Heisenberg model with $J_z/J_{xy} = 0.1$ for $D_z = 2$. The SU leads to slightly higher energies than the FFU, whereas the CU yields similar results as the FFU. For the local magnetic moment m , shown in Fig. 3(b), the deviation between the SU and FFU is more pronounced. Also here, the CU gives a significant improvement upon the SU result, with slightly larger values compared to the FFU result at large bond dimensions.

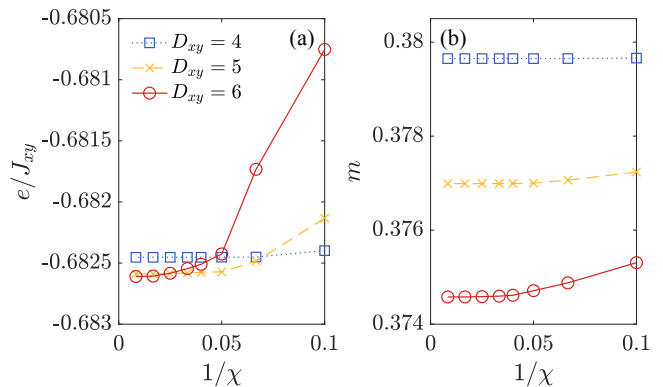


FIG. 4. Convergence as a function of χ for $D_{xy} = 4 - 6$ and $D_z = 2$. The coupling strength is $J_z/J_{xy} = 0.1$. (a) The energy per site e in units of J_{xy} . (b) Local magnetic moment m .

II. ACCURACY OF THE LCTM CONTRACTION

The accuracy of the LCTM contraction is controlled by both the boundary bond dimension χ of the CTM environment tensors as well as the number of untruncated interlayer connections that are kept in the center of the network. In this section, we analyze the dependence of the results on these parameters. We also examine alternative approaches for the $D_z > 1$ to $D_z = 1$ truncation performed away from the center.

A. Convergence in χ

In Fig. 4(a) we show the energy per site, e , for $J_z/J_{xy} = 0.1$ as a function of $1/\chi$ for different values of D_{xy} and $D_z = 2$. Convergence is reached at sufficiently large χ , where a higher χ is needed for larger D_{xy} for an accurate evaluation, as expected. Interestingly, we find that an increase in D_z does not require a larger χ to converge. Similar observations can be made for the local magnetic moment m in Fig. 4(b). For the results in the main text, χ is chosen sufficiently large such that finite- χ errors are negligible.

B. Interlayer connectivity

The number of untruncated $D_z > 1$ interlayer connections is another parameter controlling the accuracy of the LCTM method. The results in the main text have been obtained by just keeping a single connection in the center for one-site observables and interlayer two-site observables, and two connections for intralayer two-site observables. Here we present a comparison to a different scheme, in which we also keep the interlayer connections on the tensors neighboring the (two) central one(s). In practice, this can be implemented by absorbing tensors

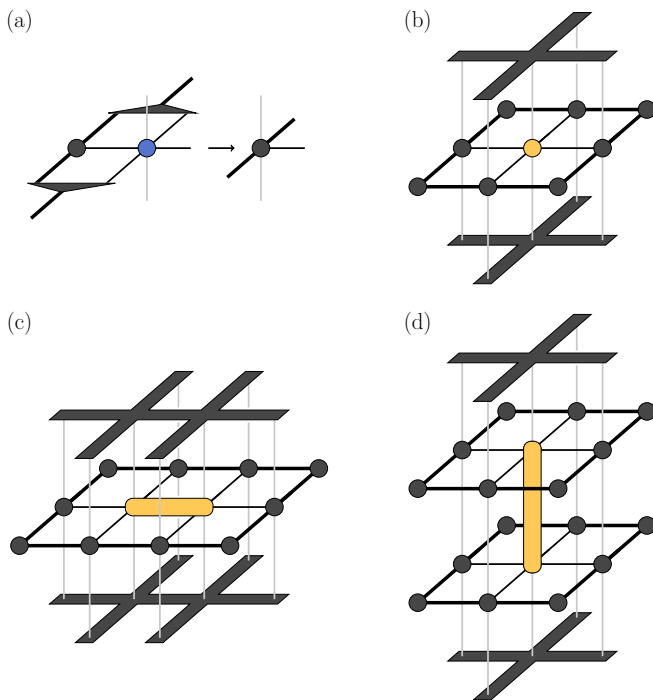


FIG. 5. Final diagrams obtained for the LCTM contraction with central and nearest-neighbor interlayer connections untruncated. The yellow tensors indicate the contraction of bra- and ket-tensors with an operator in between. (a) At the final CTM step, a tensor with untruncated interlayer connections is absorbed into the environment. (b) Computation of a one-site observable. (c) Computation of an intraplane two-site observable. (d) Computation of an interplane two-site observable.

with $D_z > 1$ into the environment tensors at the final CTM step, as depicted in Fig. 5(a). Figures 5(b-d) show the diagrams to evaluate a one-site observable, an intraplane two-site observable, and an interplane two-site observable, respectively. We call this scheme the star LCTM. It has the advantage that more of the interlayer correlations are taken into account, however, at the expense of a significantly higher contraction cost.

In Fig. 6(a) results for the nearest-neighbor spin-spin correlator in the intraplane direction are shown, using different contraction schemes to evaluate them. The tensors have been obtained for $J_z/J_{xy} = 0.1$ using the FFU imaginary time evolution based on the standard LCTM scheme. Besides the standard and star LCTM approach, we also include data from the 2D CTM in which no interlayer connections are kept (i.e. also the connection on the central tensor is truncated to $D_z = 1$), and from the full 3D contraction (SU+CTM) which we take as reference values. We observe that without the interlayer connections (2D CTM) the deviation from the SU+CTM result is relatively large, whereas both the standard and star LCTM show a close agreement with the full 3D contraction.

Figure 6(b) shows results in the interlayer direction.

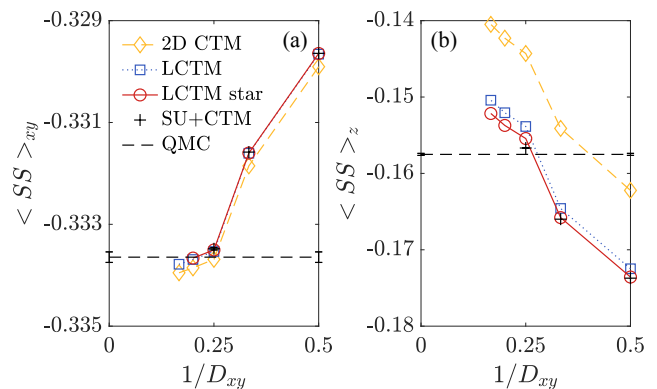


FIG. 6. Contraction results for the nearest-neighbor spin-spin correlators obtained with a 2D CTM, standard LCTM, and star LCTM with $J_z/J_{xy} = 0.1$ as a function of $1/D_{xy}$ and with $D_z = 2$. For comparison, a full 3D contraction (SU+CTM) and extrapolated QMC results are provided. (a) Nearest-neighbor spin-spin correlator in the intraplane direction $\langle SS \rangle_{xy}$. (b) Nearest-neighbor spin-spin correlator in the interplane direction $\langle SS \rangle_z$.

The deviation from the SU+CTM result is larger here with the standard LCTM scheme, although it performs much better than the 2D CTM. A significant improvement is obtained by using the star LCTM, with a close agreement to SU+CTM for $D_{xy} = 2$ and 3. For larger D_{xy} we expect that the results can be further improved by keeping even more interlayer connections.

C. Alternative layer decoupling approaches

A key step in the LCTM method is the decoupling of the layers away from the center, which for the results in the main text is done by a FU truncation to $D_z = 1$. In this section, we compare several alternative local truncation approaches to the FU results.

The first alternative we consider is to trace out the bonds in the z-direction by connecting the respective bonds of the iPEPS tensors in the bra- and in the ket-layers. On these bonds, we include the corresponding singular value matrices as an effective environment approximation, in the same spirit as done in the CU approach. Another option we test is the SU truncation based on performing a local SVD, which is equivalent to the initial truncation used in the FU approach. Finally, we also consider a CU truncation based on the larger local 3×3 environment shown in Fig. 2(d).

Figure 7(a) shows results for the energy per site, e , as a function of $1/D_{xy}$ and $D_z = 2$ at $J_z/J_{xy} = 0.1$. Here we find that the alternative truncation approaches show a good agreement with the FU layer decoupling scheme. For the $D_z = 3$ case, presented in Fig. 7(b), however, the scheme based on tracing out the interlayer connections and the SU truncation both give a significant underestimation of the energy compared to FU. Although the CU

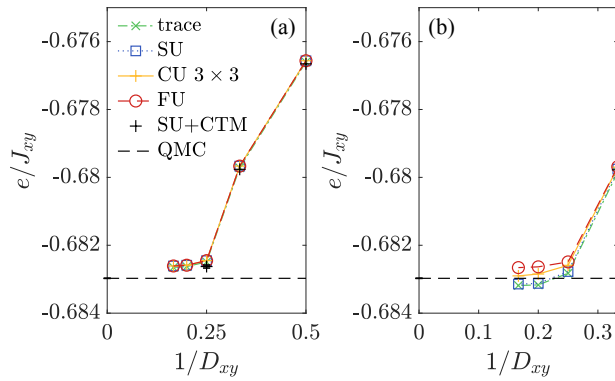


FIG. 7. Energy per site as a function of $1/D_{xy}$ with $J_z/J_{xy} = 0.1$ for alternative layer decoupling approaches based on tracing out the z-bond, a SU truncation, and a CU truncation using a 3×3 cluster size compared to a FU truncation. For reference, a SU+CTM contraction and an extrapolated QMC result are provided as well. (a) $D_z = 2$. (b) $D_z = 3$.

3×3 truncation performs better, it yields values that are too small as well. These results indicate that performing an accurate truncation is important, at least for $D_z > 2$, and they motivate the use of the computationally more expensive FU truncation in the main text.

-
- [1] J. Jordan, R. Orús, G. Vidal, F. Verstraete, and J. I. Cirac, Phys. Rev. Lett. **101**, 250602 (2008).
 [2] H. N. Phien, J. A. Bengua, H. D. Tuan, P. Corboz, and R. Orús, Phys. Rev. B **92**, 035142 (2015).
 [3] M. Lubasch, J. I. Cirac, and M.-C. Bañuls, Phys. Rev. B **90**, 064425 (2014).
 [4] H. C. Jiang, Z. Y. Weng, and T. Xiang, Phys. Rev. Lett. **101**, 090603 (2008).
 [5] L. Wang and F. Verstraete, arXiv:1110.4362 [cond-mat.str-el] (2011).
 [6] M. Lubasch, J. I. Cirac, and M.-C. Bañuls, New J. Phys. **16**, 033014 (2014).
 [7] J. Dziarmaga, Phys. Rev. B **104**, 094411 (2021).